International Journal of Architectural, Civil and Construction Sciences
ISSN: 2415-1734
Vol:13, No:9, 2019

Finite Element Approach to Evaluate Time Dependent Shear Behavior of Connections in Hybrid Steel-PC Girder under Sustained Loading

Mohammad Najmol Haque, Takeshi Maki, Jun Sasaki

***Abstract*—**Headed stud shear connections are widely used in the junction or embedded zone of hybrid girder to achieve whole composite action with continuity that can sustain steel-concrete interfacial tensile and shear forces. In Japan, Japan Road Association (JRA) specifications are used for hybrid girder design that utilizes very low level of stud capacity than those of American Institute of Steel Construction (AISC) specifications, Japan Society of Civil Engineers (JSCE) specifications and EURO code. As low design shear strength is considered in design of connections, the time dependent shear behavior due to sustained external loading is not considered, even not fully studied. In this study, a finite element approach was used to evaluate the time dependent shear behavior for headed studs used as connections at the junction. This study clarified, how the sustained loading distinctively impacted on changing the interfacial shear of connections with time which was sensitive to lodging history, positions of flanges, neighboring studs, position of prestress bar and reinforcing bar, concrete strength, etc. and also identified a shear influence area. Stud strength was also confirmed through pushout tests. The outcome obtained from the study may provide an important basis and reference data in designing connections of hybrid girders with enhanced stud capacity with due consideration of their long-term shear behavior.

***Keywords*—**Finite element approach, hybrid girder, headed stud shear connections, sustained loading, time dependent shear behavior.

I. Introduction

COMPOSITE structures have some unique characteristics as they can take the full advantage of the properties of steel and concrete by resisting tensile and compressive forces. This also can double the flexural strength and stiffness as well as can reduce the span to depth ratio with consequent cost savings in real structural construction [1], [2]. Due to such advantageous uses, composite construction has gained popularity over last few decades and composite bridges have been designed for greater span lengths which were not achieved previously with ordinary materials [3]. The hybrid steel-concrete girder system uses the lighter steel girder and the cheaper concrete girder that provides an economical solution [4] and considering the longitudinal compositions, prestressed concrete (PC) girders instead of concrete girders are preferred because of high stiffness and durability [5]. Shinozaki et al. adopted an innovative hybrid girder, intended to join steel girder with that of PC girder applicable for a span, both sides of which, there exist same number of steel girder and PC girder. Fig. 1 (a) presents such hybrid girder. Here, steel girder is embedded into PC girder and embedded part is known as junction [6]. The continuity in the junction must be achieved to resist tensile and shear forces at steel-concrete interface [1], [2]. Most commonly, headed stud shear connections are used for that purpose with many advantages including rapid installation, strength, stiffness, high ductility and enhanced shear resistance with dowel action [7]-[9]. Shinozaki et al. devised the junction of hybrid girder shown in Fig. 1 (b) with headed stud shear connections [6].

Some design specifications and codes including AISC Manual [10], EURO code [11], JRA [12] and JSCE [13] adopted formulae to determine headed stud strength for designing connections.

The JRA specifications are used for hybrid girder design in Japan [14] and stud capacity as per the JRA specifications ranges from 0.12 times to AISC specifications, 0.13 times to JSCE specifications and 0.22 times to EURO code, as summarized in Table I. Hence, as per current design specifications, the nominal shear force carried by the connector remained with limited value than its actual capacity. Thus, the shear behavior under the influence of sustained external loads with time effects is neither considered because of its low design force level nor has been fully studied yet [15]. But, if time dependent behavior is not predicted exactly, then stud-concrete interfacial deformation due to sustained shear force may lead to over-deflection with ultimate reduction in service life. At the same time, as JRA specifications remained with a substantial gap with others, it requires detailed investigation to materialize the optimum uses of stud capacity in design of connections for real structure applications.

Based on the afore-mentioned literature and stated situation, sustained loading tests were conducted with different time exposure on hybrid steel-PC girder specimens with headed stud connections. Then, a finite element (FE) approach was used to evaluate the time dependent shear behavior for those connections. The results clarified that sustained loading has distinctive impact on changing stud level interfacial shear with time and identified a shear influence area for specimen under this study. Stud shear strength was also confirmed through

Mohammad Najmol Haque is with the Structural Material Laboratory, Department of Civil and Environmental Engineering, Saitama University, Japan (corresponding author, e-mail: engrnajmol24@ yahoo.com).

Takeshi Maki is with the Structural Material Laboratory, Department of Civil and Environmental Engineering, Saitama University, Japan (e-mail: maki@mail.saitama-u.ac.jp).

Jun Sasaki was with the Structural Material Laboratory, Department of Civil and Environmental Engineering, Saitama University, Japan. He is now with the Kajima Corporation, Japan (e-mail: jsasaki102@gmail.com).

pushout tests to assess its optimum uses in real structural construction rather than using of very limited capacity.

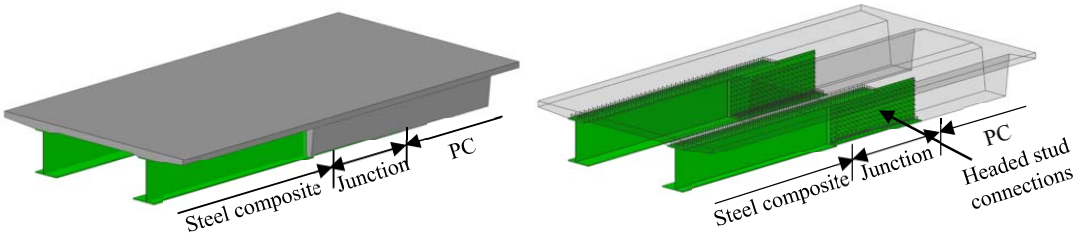

(a) Hybrid girder (b) Headed stud connections in junction

Fig. 1 Hybrid girder and junction

TABLE I
HEADED STUD SHEAR STRENGTH AS PER DIFFERENT SPECIFICATIONS AND CODES

Headed stud				Concrete		Headed stud shear strength (kN)			
Diameter (mm)	Height (mm)	Area (mm^2)	Tensile strength fu (MPa)	Desired compressive strength (MPa)	Elastic Modulus Ec (MPa)	JRA (allowable shear)	EURO Code 4 (design shear)	JSCE (design shear)	AISC (nominal shear)
13	60	132.73	473	33	27000	8	37	61	63

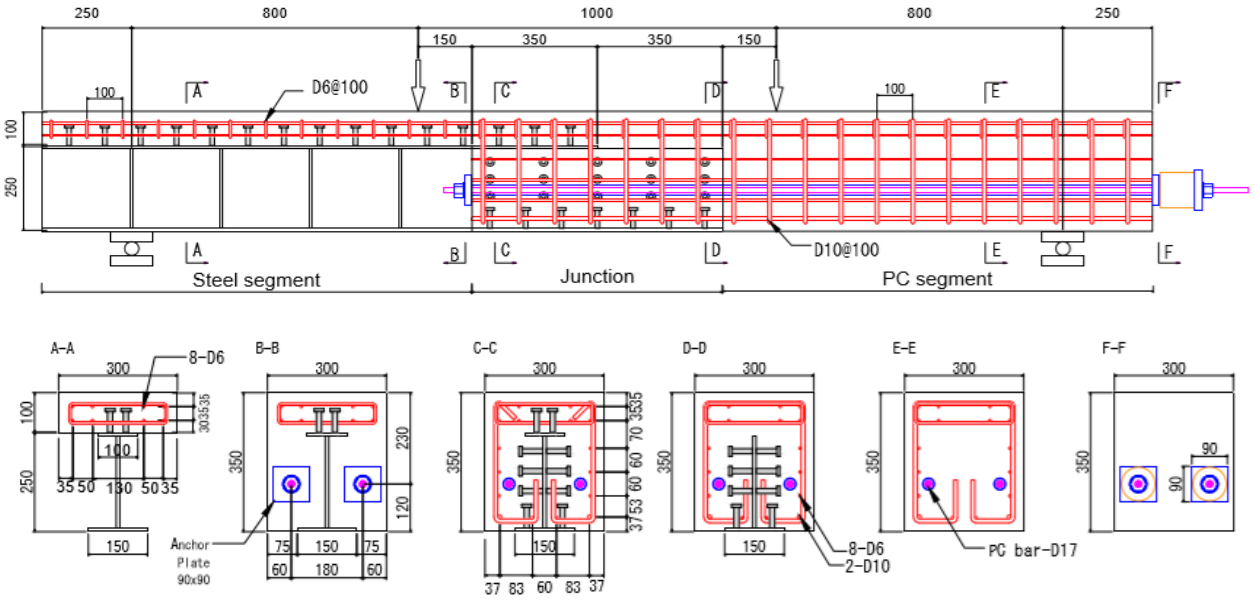

(a) Geometry and sectional details of girder specimen (unit: mm)

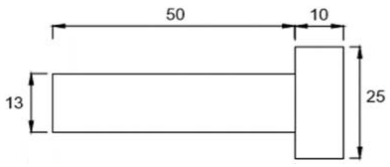

(b) Shape and size of stud (unit: mm)

Fig. 2 Hybrid girder specimen details: (a) Geometry and sectional details; (b) Shape and size of stud

II. DESIGN OF SPECIMEN

A. Geometry

To investigate the time dependent shear behavior, a scaled down hybrid steel-PC girder of a real bridge was designed as shown in Fig. 2. This hybrid girder composed of steel composite girder at one side and PC girder at another side. Steel composite segment was designed as a compact section as per JSCE standard specifications for hybrid structures 2014

[16] with a design load of 80 kN. PC segment was designed with a design load of 60 kN so that with a 195-kN prestressing load, the compression stress at the lower fiber of concrete will be neutralized by the applied decompressive design load [17]. The headed stud connections at the shear span of upper flange was designed as to sustain the axial force due to the moment for applied design load. In junction segment, the same stud connections as that of the real bridge was used. The stud capacity for designing the connections was determined as per the JSCE standard specifications for steel and composite structures 2009 [13]. Considering the geometry of girder specimen, pushout test specimen was designed as to confirm the stud capacity as used in design. Pushout test specimen details are presented in Fig. 3. Two scaled down simply supported girder specimen having identical cross-section and span were prepared and tested, referred as G-I to II. Three pushout test specimens with identical cross section were prepared and tested, referred as P-I to III.

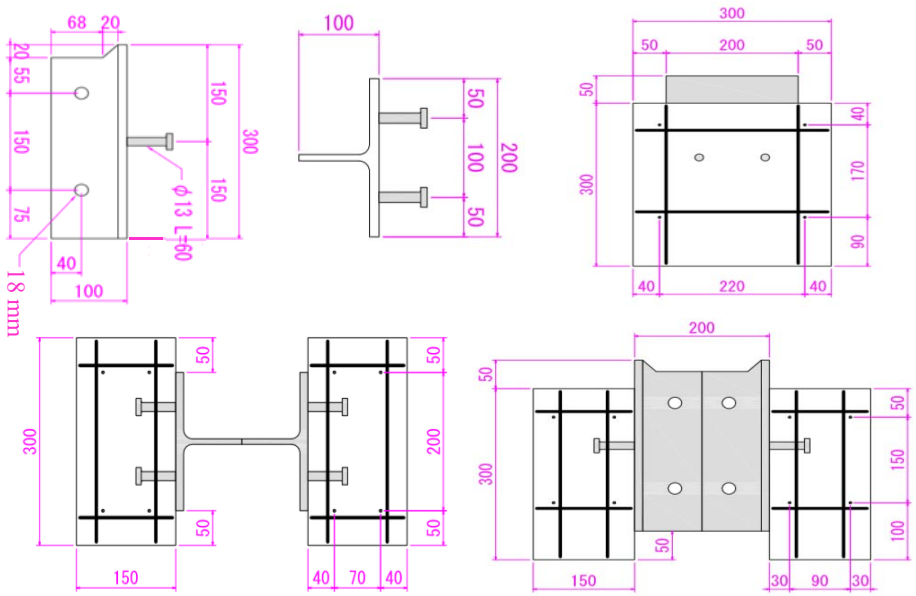

Fig. 3 Pushout test specimen details

TABLE II
CONCRETE MIX PROPORTIONS AND STRENGTH

Specimen	Concrete mix proportions (kg/m^3)						Concrete Compressive strength		Type of cement
-	W/C Ratio (%)	Cement	Water	Coarse aggregate	Fine aggregate	Air entraining agent	Strength (Mpa)	Age from casting (days)	-
G-I	44.5	394	175	990	767	5.12	54.8	46	Early strength Portland cement
G-II						3.94	36.0	14	
P-I	44.5	394	175	990	767	3.94	36.0	14	
P-II							39.92	28	
P-III							41.62	42	

B. Material Properties

The instantaneous compressive strength of concrete at different ages for girder specimens and pushout specimens were obtained through standard cylinder (200 mm high with a diameter of 100 mm) tests. The material properties for concrete, steel girder section, prestressing bars and headed stud connectors are summarized in Tables II and III.

III. TEST SETUP

A. Test Specimens' Sensor Layout and Loading History

For taking the measurements, sensors were placed at suitable locations on girder specimens and pushout specimens as illustrated in Fig. 4. Pure bending moment condition was applied to achieve the whole composite action at the junction. Therefore, two vertical loads were applied in a simply supported girder specimen as shown in Fig. 4 (a). After the introduction of prestressing force, G-I and G-II both were subjected to sustained loading (application of vertical load for a specific time duration) of different time duration as summarized in Table IV. After two days since the application of prestressing, G-I was under sustained loading of 30 kN, 40 kN, 50 kN, 60 kN and 80 kN for a period of 14 days each. In case of G-II, after introduction of prestress force, it was only under prestress for 14 days and then was under 60 kN sustained load for 28 days more. Assumption was that the shear force behavior of first 14 days for G-II will reflect the variations due to the environmental effects, then next 28 days to assess whether the same shear force behavior continued for longer period under 60 kN as similar to G-I. For pushout

specimens, the cyclic loading was conducted with 5% shear force intervals until the specimen failure as to confirm the shear capacity of stud used in connections of hybrid girder.

B. Environmental Conditions

For G-II, temperature was measured to distinct the behavior due to sustained loading with that of due to the variations of environmental conditions. The variations of temperature with time, illustrated in Fig. 5, in which, time represents the time from prestressing of specimens.

TABLE III
SUMMARY OF MATERIAL PROPERTIES

Specimen	Yield strength *fy* (Mpa)				Tensile strength *fu* (Mpa)			
-	Steel web	Steel flange	Prestress bar	Stud	Steel web	Steel flange	Prestress bar	Stud
G-I	429	383	1198	408	550	535	1290	473
G-II	396	347	1189	440	536	446	1277	487
P-I								
P-II	396	347	-	440	536	446	-	487
P-III								

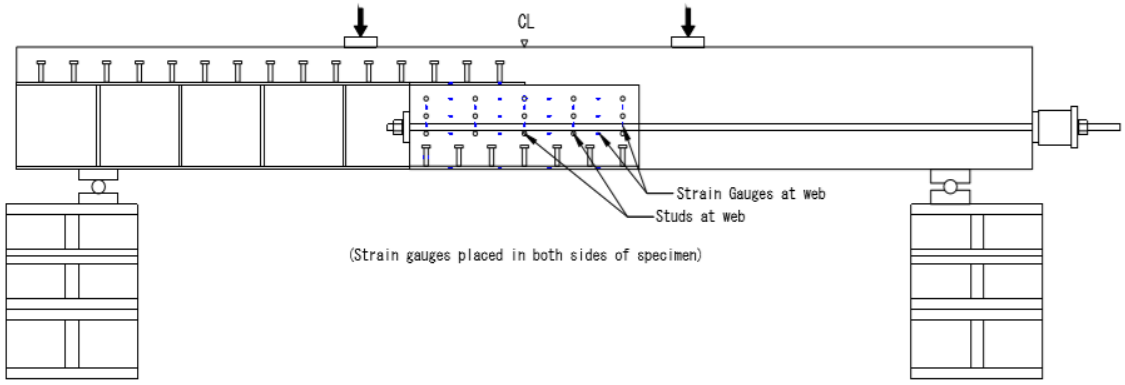

(a) Loading arrangement and layout of strain gauges and studs at web in junction of hybrid girder

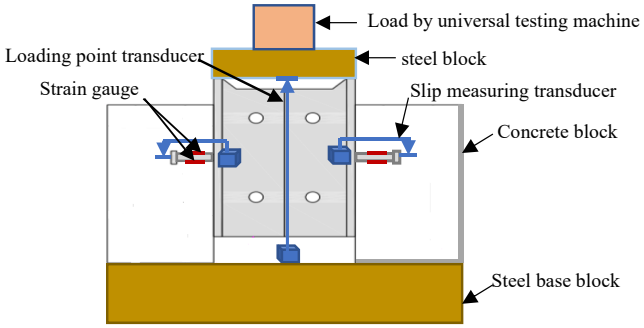

(b) Loading arrangement and layout of sensors on pushout specimens

Fig. 4 Loading and sensors arrangement: (a) Hybrid girder; (b) Pushout specimens

TABLE IV
SUMMARY OF GIRDER SPECIMENS LOADING HISTORY

Specimen	Time of loading (Days)							Loading type
-	Prestress (195 kN)	30 kN	40 kN	50 kN	60 kN	80 kN	Final loading	-
G-I	72	14	14	14	14	14	72nd day	Sustained loading
G-II	42	-	-	-	28	-	42nd day	

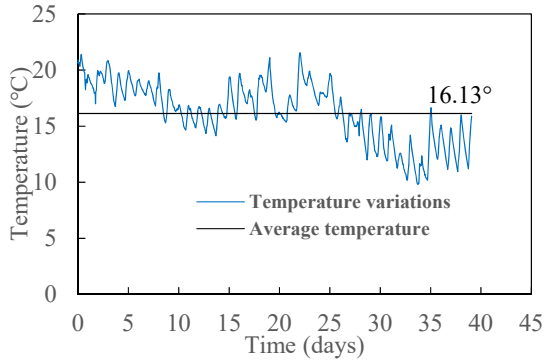

Fig. 5 Environmental conditions variations

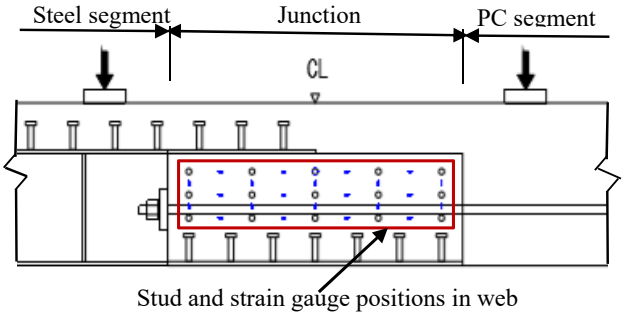

(a) Stud and strain gauges positions in web

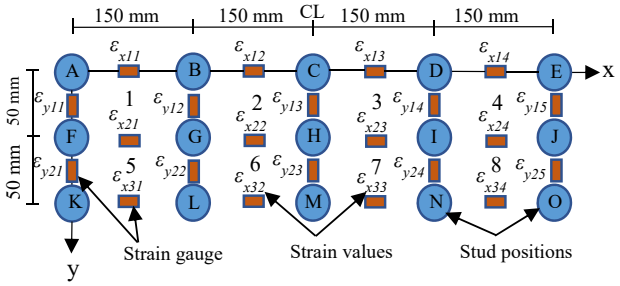

(b) Detailing of element and nodal studs

Fig. 6 Junction details

IV. FE Approach to Evaluate Shear Force on Connections

To evaluate the time dependent shear behavior in headed stud connections at junction part, an FE approach as mentioned in earlier research [18], [19] was used to evaluate the shear forces acting on the stud connections in web. The stud and strain gauges positions in web of junction part are shown in Fig. 6 (a) and a closed-up view of that is further illustrated in Fig. 6 (b). Each stud position marked alphabetically was considered as a nodal point and 4 nodal studs constituted an element from 1 to 8 as shown. The nodal stud A was placed in origin assuming the influence of local deformation and crack as small comparing to others. For FE analysis, force and displacement arrangement followed as, u_{ij} = x directional axial displacement; v_{ij} = y directional axial displacement; f_{xij} = x directional axial shear force; f_{yij} = y directional axial shear force. The arrangement of force and displacement vectors at nodal points of element 1 is illustrated in Fig. 7.

For calculation of the time dependent shear force acting on each stud due to sustained loading, (1) was considered as element stiffness equation.

$$[k]^e\{u\}^e = \{f\}^e \tag{1}$$

where, $[k]^e$ = stiffness matrix; $\{u\}^e$ = $d$isplacement vector; $\{f\}^e$ = force vector. For the calculation of force vector $\{f\}^e$ at the node as shown in Fig. 7, the stiffness matrix $[k]^e$ and the displacement vector $\{u\}^e$ were needed to be determined. The displacement vector $\{u\}^e$, the relative nodal displacement was calculated by multiplying the strain obtained experimentally from the strain gauge placed between two nodes by the length between them, assuming the uniform strain distribution between the two adjacent nodes. Stiffness matrix $[k]^e$ was determined as per (2).

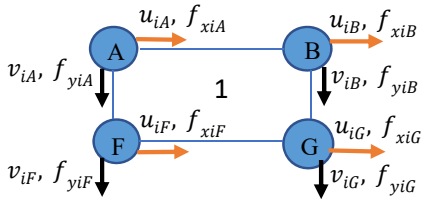

Fig. 7 Forces and displacement vectors at nodal points of element 1

$$[k]^e = \int_{-1}^{1}\int_{-1}^{1}[B]^T[D][B]|J|dsdt \tag{2}$$

where, $[B]$ and $[D]$ were matrixes and $|J|$ was the Jecobian matrix.

Since the plate thickness was small relative to the x and y axis, the plane stress formulae were adopted. If the stress vector is defined as $\{\sigma\}$ and the strain vector as $\{\varepsilon\}$ then, the following expression was considered as shown in (3). Therefore, the $[D]$ matrix, a symmetric matrix that relates stress vector and strain vector, expressed as shown in (4).

$$\{\sigma\} = [D]\{\varepsilon\} \tag{3}$$

$$[D] = \frac{E}{1-\nu^2}\begin{bmatrix} 1 & \nu & 0 \\ \nu & 1 & 0 \\ 0 & 0 & \frac{1-\nu}{2} \end{bmatrix} \tag{4}$$

Regarding matrix $[B]$, relational expression of strain and displacement (u, v) in plane stress expressed in (5) and accordingly $[B]$, expressed in (6). Here, Ni known as shape function which was defined with a local coordinate system (s, t) of -1 to +1 for an element other than a triangle, that represented the displacement and coordinate of an arbitrary point in the element. Concept of a shape function illustrated in Fig. 8 and a 4-node quadrilateral element was used in this

study as expressed in (7). The partial differential of (7) with respect to (s,t) led to an expression shown in (8).

$$\{\varepsilon\} = \begin{Bmatrix} \varepsilon_x \\ \varepsilon_y \\ \gamma_{xy} \end{Bmatrix} = \begin{bmatrix} \frac{\partial N_i}{\partial x} & 0 \\ 0 & \frac{\partial N_i}{\partial y} \\ \frac{\partial N_i}{\partial y} & \frac{\partial N_i}{\partial x} \end{bmatrix} \begin{Bmatrix} u_1 \\ u_2 \\ u_3 \\ u_4 \\ v_1 \\ v_2 \\ v_3 \\ v_4 \end{Bmatrix} = [B] \begin{Bmatrix} u_i \\ v_i \end{Bmatrix} \quad (5)$$

$$[B] = \begin{bmatrix} \frac{\partial N_i}{\partial x} & 0 \\ 0 & \frac{\partial N_i}{\partial y} \\ \frac{\partial N_i}{\partial y} & \frac{\partial N_i}{\partial x} \end{bmatrix} = \begin{bmatrix} \frac{\partial N_1}{\partial x} & \frac{\partial N_2}{\partial x} & \frac{\partial N_3}{\partial x} & \frac{\partial N_4}{\partial x} & 0 & & & \\ 0 & & & & \frac{\partial N_1}{\partial y} & \frac{\partial N_2}{\partial y} & \frac{\partial N_3}{\partial y} & \frac{\partial N_4}{\partial y} \\ \frac{\partial N_1}{\partial y} & \frac{\partial N_2}{\partial y} & \frac{\partial N_3}{\partial y} & \frac{\partial N_4}{\partial y} & \frac{\partial N_1}{\partial x} & \frac{\partial N_2}{\partial x} & \frac{\partial N_3}{\partial x} & \frac{\partial N_4}{\partial x} \end{bmatrix} \quad (6)$$

$$\begin{cases} N_1(s,t) = \frac{1}{4}(1-s)(1-t) \\ N_2(s,t) = \frac{1}{4}(1+s)(1-t) \\ N_3(s,t) = \frac{1}{4}(1+s)(1+t) \\ N_4(s,t) = \frac{1}{4}(1-s)(1+t) \end{cases} \quad (7)$$

$$\begin{cases} \frac{\partial N_1}{\partial s} = -\frac{1}{4}(1-t), \ \frac{\partial N_2}{\partial s} = \frac{1}{4}(1-t) \\ \frac{\partial N_3}{\partial s} = \frac{1}{4}(1+t), \ \frac{\partial N_4}{\partial s} = -\frac{1}{4}(1+t) \\ \frac{\partial N_1}{\partial t} = -\frac{1}{4}(1-s), \ \frac{\partial N_2}{\partial t} = -\frac{1}{4}(1+s) \\ \frac{\partial N_3}{\partial t} = \frac{1}{4}(1+s), \ \frac{\partial N_4}{\partial t} = \frac{1}{4}(1-s) \end{cases} \quad (8)$$

The matrix $[B]$ in (6) contained $\partial Ni/\partial x$ and $\partial Ni/\partial y$ of (x,y) coordinate system, whereas the shape function contained Ni in (s,t) coordinate system which cannot be partially differentiated with respect to (x,y). Therefore, a Jacobian [J] matrix was introduced as shown in (9) where, $x_1 \sim x_4$ and $y_1 \sim y_4$ are the nodal coordinate of an element. The relationship between $\partial Ni/\partial x$, $\partial Ni/\partial y$ and $\partial Ni/\partial s$, $\partial Ni/\partial t$ is expressed in (10). Using (9) and (10) and assigning the expressions in (6), the matrix $[B]$ was obtained.

$$[J] = \begin{bmatrix} \frac{\partial x}{\partial s} & \frac{\partial y}{\partial s} \\ \frac{\partial x}{\partial t} & \frac{\partial y}{\partial t} \end{bmatrix} = \begin{bmatrix} \frac{\partial N_1}{\partial s} & \frac{\partial N_2}{\partial s} & \frac{\partial N_3}{\partial s} & \frac{\partial N_4}{\partial s} \\ \frac{\partial N_1}{\partial t} & \frac{\partial N_2}{\partial t} & \frac{\partial N_3}{\partial t} & \frac{\partial N_4}{\partial t} \end{bmatrix} \begin{bmatrix} x_1 & y_1 \\ x_2 & y_2 \\ x_3 & y_3 \\ x_4 & y_4 \end{bmatrix} \quad (9)$$

$$\begin{Bmatrix} \frac{\partial N_i}{\partial x} \\ \frac{\partial N_i}{\partial y} \end{Bmatrix} = [J] \begin{Bmatrix} \frac{\partial N_i}{\partial s} \\ \frac{\partial N_i}{\partial t} \end{Bmatrix} = \frac{1}{|J|} \begin{bmatrix} \frac{\partial y}{\partial t} & -\frac{\partial y}{\partial s} \\ -\frac{\partial x}{\partial t} & \frac{\partial x}{\partial s} \end{bmatrix} \begin{Bmatrix} \frac{\partial N_i}{\partial s} \\ \frac{\partial N_i}{\partial t} \end{Bmatrix} \quad (10)$$

In order to obtain the rigidity matrix of (2), the Gaussian integration was introduced to calculate the integral value in the coordinates called Gauss points with the integral ranged from –1 to +1. Since, two-point integration and three-point integration are widely used in the FE method, here three-point integration was used as illustrated in (11) with values of $c_1 = 5/9$, $c_2 = 8/9$, $c_3 = 5/9$, $s_1 = -\sqrt{3/5}$, $s_2 = 0$ and $s_3 = \sqrt{3/5}$.

$$\int_{-1}^{1} f(s)ds \approx c_1 f(s_1) + c_2 f(s_2) + c_3 f(s_3) \quad (11)$$

As per the previous Gaussian integral, assuming $f(s,t) = [B]^T[D][B]|J|$, the following expression was achieved as shown in (12) where, subscripts i,j refer to the value calculated at each Gaussian point.

$$[k]^e = \sum_{i=1}^{3}\sum_{j=1}^{3} c_i c_j [B]_{ij}^T [D][B]_{ij}|J|_{ij} \quad (12)$$

Each element in this analysis consisted of 150 mm arm length in horizontal direction and 50 mm in vertical direction with same material, hence same stiffness matrix was obtained for element 1 to 8. By substituting the value of element stiffness matrix in (1), the forces acted on studs (nodes) of each element were obtained. Therefore,

$$[8 \times 8]^e \begin{Bmatrix} u_{iA} \\ u_{iB} \\ u_{iG} \\ u_{iF} \\ v_{iA} \\ v_{iB} \\ v_{iG} \\ v_{iF} \end{Bmatrix} = \begin{Bmatrix} fx_{iA} \\ f_{xiB} \\ f_{xiG} \\ f_{xiF} \\ f_{yiA} \\ f_{yiB} \\ f_{yiG} \\ f_{yiF} \end{Bmatrix}$$

As, (1) applicable for stiffness matrix for each element, the overall stiffness matrix for 15 nodal studs was required to determine the shear force acted on each stud. Overall stiffness matrix $[K]$ (the number of nodes x degrees of freedom) of 15 studs with two degrees of freedom led to a 30 x 30 stiffness matrix as shown herein.

$$[30 \times 30] \begin{Bmatrix} u_A \\ u_B \\ \vdots \\ u_N \\ u_o \\ v_A \\ v_B \\ \vdots \\ v_N \\ v_o \end{Bmatrix} = \begin{Bmatrix} f_{xA} \\ f_{xB} \\ \vdots \\ f_{xN} \\ f_{xo} \\ f_{yA} \\ f_{yB} \\ \vdots \\ f_{yN} \\ f_{yo} \end{Bmatrix}$$

Hence, the shear force (f_x and f_y) at each stud (nodal point) was obtained using stiffness matrix and nodal displacement values as calculated by the method already mentioned above.

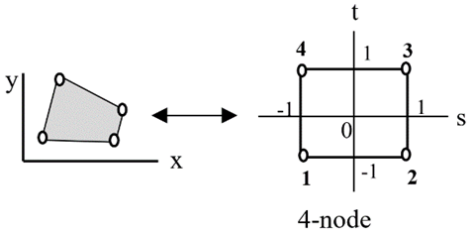

Fig. 8 Shape function

V. Results and Discussions

The overall time dependent shear behavior of connections under sustained loading and test results on confirmation of the

shear strength of stud through pushout tests will be discussed in following sections.

A. Shear Behavior of Connections under Sustained Loading

Based on the experimental data, an FE analysis, as already mentioned in the preceding section was conducted and results thus obtained are presented in Figs. 9 and 10. For G-I, sustained loading of 30 kN, 40 kN, and 50 kN were below the design load that did not produce whole composite action through connections, hence shear behavior only under sustained design load (60 kN and 80 kN) discussed here. It was observed that, due to introduction of prestress force, three stud layers (upper, middle and lower) were mostly under compressive shear force which was the likely case as they were below the neutral axis. Studs in upper layer also faced y-axial tensile shear force because of flange position that covered half of the area that influenced the stud concrete interaction resulted with such shear force direction. Few other studs also showed tensile shear force due to the positions of neighboring studs or reinforcement that might have influenced the behavior. Just after introduction of 60 kN load, due to flexure induced tensile stress below the neutral axis, the instantaneous shear force increased in magnitude in both directions and when the same load sustained for 14 days, then shear force showed further increment in magnitude with a sign of sustained loading effects. The upper and lower layer of studs mostly experienced the tensile shear force whereas the lower layer experienced the compressive shear force. As the lower layer was very close to both prestressing bar and studs at lower flange, due to which this layer faced restraining force from them resulting in compressive shear force. When the load level reached to 80 kN, the instantaneous shear force increased in magnitude in both directions, comparatively with small incremental value that happened in 60 kN load. Some shear force values were almost closer to that of 60 kN load, the reason of that may be the existence of flanges in upper and lower part which could carry the instantaneous bending effects as bearing force. But when the 80 kN load sustained for 14 days, shear force magnitude showed mostly incremental behavior with a clear effect of sustained loading. Few studs in different layers did not show consistent shear variations due to the reason of nearby studs, position of prestress bar, anchor plate and reinforcing bar which have influenced the behavior. It was observed that studs in three layers who remain in the area from center line to rightward region where the upper flange was terminated showed higher magnitude of shear force, whereas the region from centerline to leftward side which contain upper flange showed shear force magnitude with relatively lesser value. This clearly indicated the influence of upper flange in shear force behavior. Thus, the area where upper flange did not exist has behaved as a shear influence area where change of shear magnitude over time significantly noticed. The axial shear force parallel to girder's longitudinal axis was mostly dominating. In contrary, it seemed that upper flange actively influenced shear force magnitude normal to the girder's axis as it took a portion of flexural force as bearing force.

For G-II, almost similar shear behavior obtained for three layers of studs. As creep and shrinkage of concrete are considered as sources of time dependent behavior [20], to differentiate the effects, a comparison of shear behavior was needed. For first 14 days, G-II was kept only under prestress force without any sustained loading. Hence, the shear behavior recorded for G-II for first 14 days was assumed to be representative of shrinkage due to environmental effects, which therefore demonstrated how the behavior can be influenced over variations of environmental conditions. After that, when 60 kN load was applied and continued as sustained loading, similar behavior as that of G-I was observed with distinctive effect of sustained load although magnitude of shear force varied under same load between the two specimens. Shear influence area also observed here with the same underlying reason of previous one and shown in Fig. 11. It seemed as a bit complex phenomenon to clarify the reasons very keenly behind the variations. A very possible reason was the earlier loading history, as G-I was subjected to prestress force for 2 days, then 3 steps intermediate sustained loading (30 kN, 40 kN and 50 kN) for 42 days before 60 kN load level and specimen G-II was subjected to long time prestress force for 14 days, before 60 kN sustained load, then 28 days under that load. As earlier loading history and sustained loading time differ with each other in G- I and G-II, shear force variation over time due to sustained loading effect was not directly comparable in terms of magnitude. On the other hand, compressive strength of concrete in these two specimens differ significantly which also have influenced stud-concrete interface behavior with definite impact on variations of shear force magnitude. The shear force behavior of any stud also could change depending on how the neighboring studs behaved due to any deflection or deformation by external forces. In case of G-II, middle layer studs have been influenced less in terms of magnitude and variations of shear force comparing to upper and lower layer, which was due to the position of prestressing bar with active involvement of prestress force near to that layer. However, comparing the shear force behavior due to prestress force with that of sustained loading in G-II, it was clarified that shear due to creep (other than shrinkage) significantly dominated than that caused by shrinkage.

It was also needed to be clarified why sustained loading has impact on increasing shear magnitude at studs. When external load sustained on girder, it was flexure that induced deflection at girder and mostly influenced part was junction. Owing to this deflection, local deformations have taken place at stud-concrete vicinity as well as slip deformations also taken place at steel-concrete interface. These deformations phenomena were continued throughout the loading time which have directly influenced the shear forces acting on stud connections. This phenomenon clearly put a concern that if shear force magnitude changes increasingly over the sustained loading period at connections, then due to local deformations and slippage, overall deflections of girder would be aggravated with immediate effects of appearing cracks earlier than expected. Also, the shear force for which the connections were

designed will experience that level of force at an earlier time than predicted. This will affect the service life of the structures.

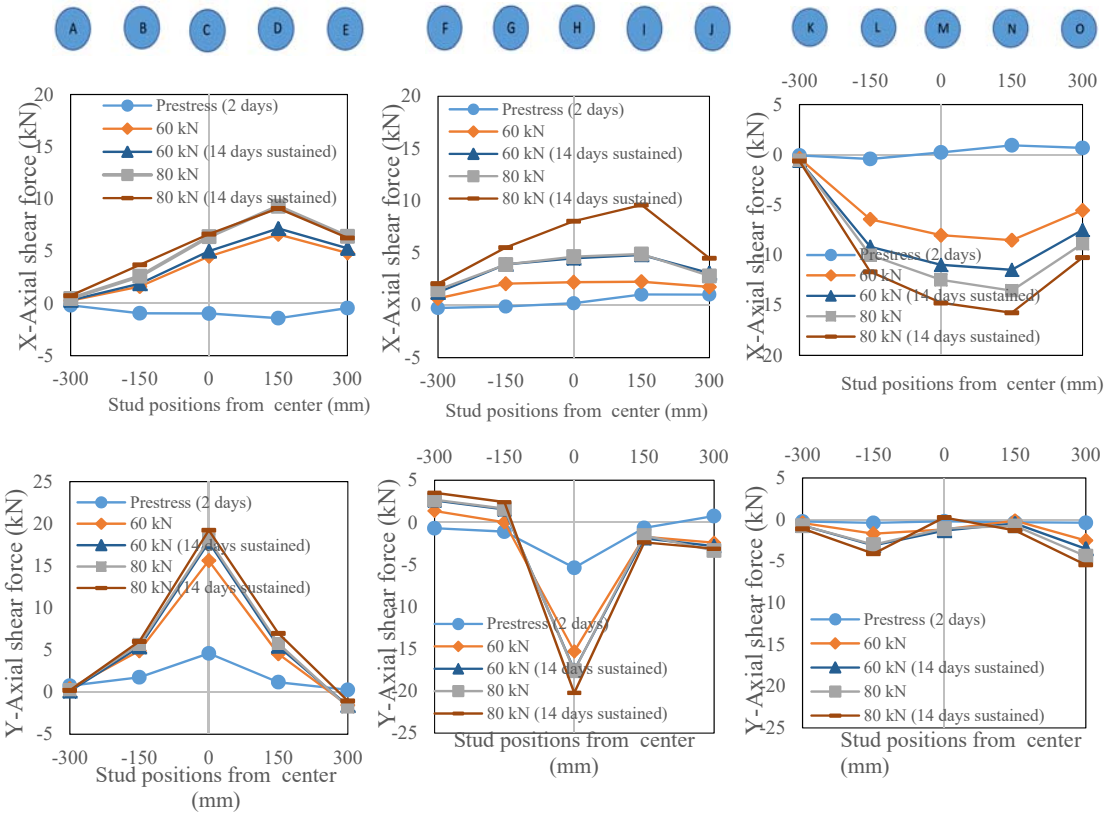

Fig. 9 Shear force behavior under sustained loading in G-I

B. Pushout Test for Confirmation of Shear Strength

Three pushout specimens of different ages and compressive strength as already mentioned in Table II, tested under cyclic loading and the shear force – slip relationship obtained for such, illustrated in Fig. 12. The vertical axis indicated the shear force per-stud obtained by dividing the applied load by the number of studs. The shear force was maximized when the slip displacement was 4.49 mm for P-I, 6.24 mm for P-II, and 14.34 mm for P-III. The degree of change in slip at maximum shear capacity varied with somewhat a higher value. As all the specimens have same material characteristics except age and compressive strength of concrete, it seemed a bit complex to differentiate the factors which were dominant in that case but most importantly it seemed compressive strength of concrete reasonably substantiated it. In case of P-I, the maximum shear capacity 50.50 kN which induced 4.49 mm slip displacement. For same shear force level, slip values for P-II were relatively smaller and for P-III were much smaller as the compressive strength of concrete was higher in these two specimens. The slip displacement at maximum shear force for P-III reached to a higher value compared with the other two, as the stud failure was observed which accumulated and sustained with such higher displacement. The shear capacity ratio as presented in Table V revealed that as the days passed, concrete gained much compressive strength and progressed to the capacity as closer to the specifications value and beyond. It is to be mentioned that, the size of the pushout specimen was chosen keeping consistent with the size of the girder specimen which was smaller than the size prescribed in specifications. Hence, with smaller size and lesser compressive strength, P-I and P-II showed less shear capacity than the specification value although after reaching a certain compressive strength, specimen achieved desired strength as reflected in P-III. However, in real structures, girder specimen will be matured enough in terms of age to gain necessary strength before subjected to field loading. Hence, it could be expected that desired strength would be achieved. In this study, sustained maximum shear force that the stud connections have experienced under 60 kN load were approximately 12 kN in G-II and 18 kN in G-I which almost 24% and 35% of experimentally confirmed strength of stud. At 80 kN sustained load, the maximum stud shear force was approximately 22 kN in G-I, which, almost 44% of experimentally confirmed strength of stud. Although maximum sustained shear force remained below 50% of stud capacity, it warrants detailed study with longer duration on how much stud capacity can be considered in design realizing the time dependent sustained loading effects on shear behavior

of connections which associated with local deformations at stud-concrete vicinity as well as deformations at steel-concrete interface.

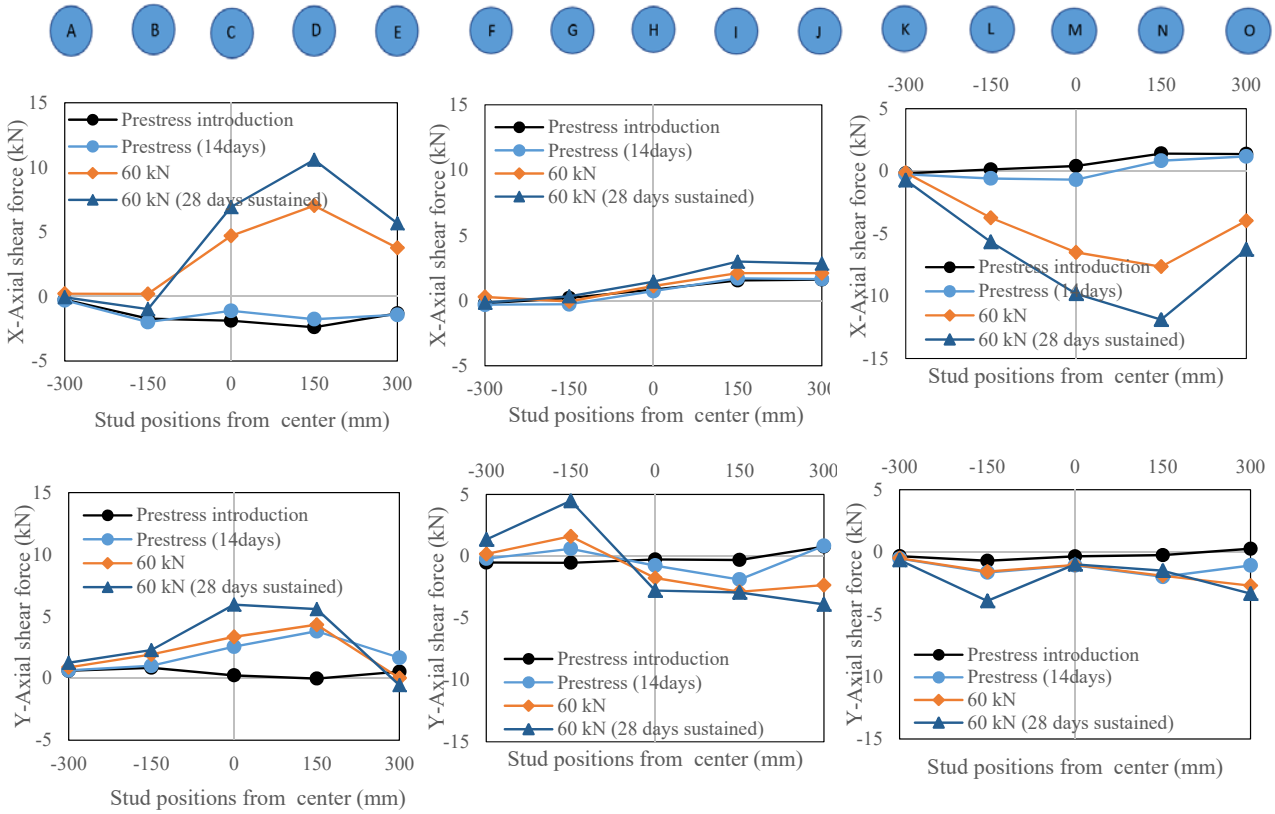

Fig. 10 Shear force behavior under sustained loading in G-II

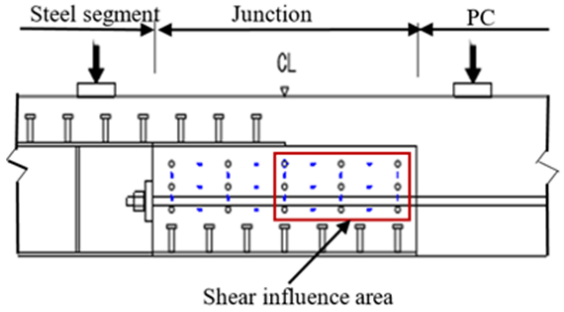

Fig. 11 Shear influence area

TABLE V
STUD CAPACITY AND FAILURE MODE

Specimen	Shear Capacity (kN)		Ratio (exp./ cal.)	Failure mode
-	Exp.	JSCE specification		-
P-I	50.50	63.04	0.80	Concrete failure
P-II	59.53	64.68	0.93	Concrete failure
P-III	72.68	64.68	1.12	Stud failure

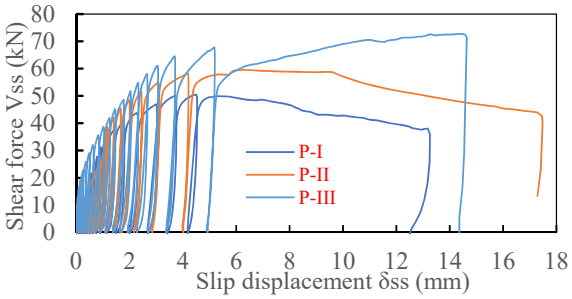

Fig. 12 Shear force and slip displacement in pushout tests

VI. CONCLUSIONS

Two scaled down hybrid girder specimens were tested with headed stud shear connections, then an FE approach was used to evaluate the time dependent shear behavior and described in this paper. The distinctive time dependent shear behavior clarified and to what extent, environmental effects can influence the behavior was also checked. The following conclusions can be drawn from the results.

(1) The results presented herein, explained that time dependent shear impact is obvious in headed stud

connections of hybrid girder that needs due consideration in design for long term serviceability. Such effect also needs to be considered for other types of connections.

(2) The reason clarified here for change of shear magnitude under sustained loading as the local deformations at stud-concrete vicinity as well as slip at steel-concrete interface that aggravate with exposure time. This time dependent shear significantly depends on earlier loading history, i.e. magnitude increases with time, position of flanges and neighboring studs, position of prestress bar and reinforcing bar, compressive strength of concrete etc. It was observed that shear due to creep significantly dominated than that caused by shrinkage.

(3) A shear influence area was also identified here. The time dependent shear tendency revealed that connections will be exposed to that level of shear force for which they were designed at an earlier time than predicted. Here, the maximum shear force experienced by stud under sustained loading accounted as less than 50% of experimentally confirmed capacity although time duration was not so long. Based on the result of present study, further study required with longer duration to obtain more detailed behavior. Then, a numerical analysis is required to validate experimental results to allow such behavior into design consideration for headed stud connections in hybrid girder.

ACKNOWLEDGMENT

The work in this paper was supported by JSPS KAKENHI (Grant in Aid for Scientific Research (B), Grant number JP15H04030) which is acknowledges here with thanks. The authors would like to acknowledge the indebtedness to Dr. Hiroo Shinozaki of Sumitomo-Mitsui Corporation for his suggestion to design the specimen as presented in his paper [6]. The authors also would like to express sincere thanks to Mr. Shota Sekimoto, a graduate student with Ms. Saki Shiiya and Mr. Takeru Suzuki, two undergraduate students of this laboratory for their support in conducting experiments.

REFERENCES

[1] D.J. Oehlers, M.A. Bradford, Composite Steel and Concrete Structural Members, Elsevier Science Ltd, 1995,

[2] J.F. Chooa, Y.C. Choib, W.C. Choic, S.W. Yoo, Behavioral characteristics of hybrid girders according to type of steel–concrete connection, Archives of civil and mechanical engineering, 19 (2019), pp. 47–62.

[3] J. Nie, C.S. Cai, Steel-Concrete Composite Beams Considering Shear Slip Effects, Journal of Structural Engineering, ASCE, April 2003, pp. 495-506.

[4] S.E. Kim, H.T. Nguyen, Evaluation of connection efficiency of hybrid steel-concrete girder using finite element approach, International Journal of Mechanical Sciences, 61 (2012), pp. 8–23.

[5] Y. Deng, G. Morcous, Efficient Prestressed Concrete-Steel Composite Girder for Medium-Span Bridges. I: System Description and Design, Journal of Bridge Engineering, ASCE, December 2013, pp. 1347-1357.

[6] H. Shinozaki, H. Asai, Y. Kaminaga, T. Maki, H. Mutsuyoshi, A study on joint of composite steel girder and PC girder using shear connecting method, Journal of Structural Engineering, JSCE, Vol.60A(2014/3), pp. 861-871.

[7] A. Prakash, N. Anandavalli, C.K. Madheswaran, J. Rajasankar, N. Lakshmanan, Three-Dimensional FE Model of Stud Connected Steel-Concrete Composite Girders Subjected to Monotonic Loading, International Journal of Mechanics and Applications, 2011 1(1), pp. 1-11.

[8] E. Allobody, Finite Element Analysis and Design of Steel and Steel-Concrete Composite Bridges, 2014.

[9] T. Anju, K.K. Smitha, Finite Element Analysis of Composite Beam with Shear Connectors, International Conference on Emerging Trends in Engineering, Science and Technology (ICETEST - 2015), Procedia Technology, 24 (2016), pp. 179 – 187.

[10] American Institute of Steel Construction, Specification for Structural Steel Buildings, 130 East Randolph Street, Suite 2000 Chicago, Illinois, 60601-6204, July 2016.

[11] European Committee for Standardization, Eurocode 4: Design of composite steel and concrete structures-Part 1-1: General rules and rules for buildings, Management Centre, rue de Stassart, 36 B-1050 Brussels, December 2004.

[12] Japan Road Association, Specifications for Highway Bridges, Part-2-Steel Bridges. Tokyo, Japan, 2002.

[13] Japan Society of Civil Engineers, Standard Specifications for Steel and Composite Structures, Tokyo, Japan, December 2009.

[14] M. Nagai, E. Yamaguchi, T. Yoda, K. Nogami, Recent trend on design and construction of steel and composite bridges in Japan, IABSE-JSCE Joint Conference on Advances in Bridge Engineering-II, Dhaka, Bangladesh, August 2010.

[15] T. Maki, R. Watanabe, Mechanical Behavior of Stud Shear Connector under Sustained Shear and Compression Forces, The Proceedings of the Thirteenth East Asia-Pacific Conference on Structural Engineering and Construction, , Hokkaido, Japan, 2013.

[16] Japan Society of Civil Engineers, Standard Specifications for Hybrid Structures 2014, Tokyo, Japan, March 2015.

[17] A.H. Nilson, D. Darwin, C.W. Dolan, Design of Concrete Structures, The Mac-Graw Hill Companies, Inc., Avenue of the Americas, New York, NY 10020, 2010.

[18] Introductory course on finite element method for marine engineers, Journal of the JIME, Vol. 49, No. 2, 2014.

[19] N. Ueda, K. Phamavanh, R. Sano, H. Nakamura, M. Kunieda, Study on Evaluation Method on Damage Region and Failure Criterion on RC Member Failed in Shear Compression by Means of Strain Index, Journal of JSCE (Material. Concrete Structures), Vol. 70, No. 1, 2014, pp. 1-18.

[20] Y. Okui, M.Nagai, Block FEM for Time-Dependent Shear-Lag Behavior in Two-I Girder Composite Bridges, Journal of Bridge Engineering, ASCE, 12(1), January/February 2007, pp. 72-79.